Computers and Concrete, *Vol. 26, No. 2 (2020) 137-150*
DOI: https://doi.org/10.12989/cac.2020.26.2.137

On static bending of multilayered carbon nanotube-reinforced composite plates

Ahmed Amine Daikh*[1,2], Ismail Bensaid[3], Attia Bachiri[4], Mohamed Sid Ahmed Houari[2], Abdelouahed Tounsi[4,5] and Tarek Merzouki[6]

[1]*Structural Engineering and Mechanics of Materials Laboratory, Department of Civil Engineering, Mascara, Algeria*
[2]*Mechanics of Structures and Solids Laboratory, Faculty of Technology, University of Sidi Bel Abbes, Algeria*
[3]*IS2M Laboratory, Faculty of Technology, Mechanical Engineering Department, Tlemcen University, Algeria*
[4]*Material and Hydrology Laboratory, Faculty of Technology, Civil Engineering Department, University of Sidi Bel Abbes, Algeria*
[5]*Department of Civil and Environmental Engineering, King Fahd University of Petroleum and Minerals, 31261, Dhahran, Eastern Province, Saudi Arabia*
[6]*LISV, University of Versailles Saint-Quentin, 10-12 Avenue de l'Europe, 78140, Vélizy, France*

(*Received March 24, 2020, Revised July 20, 2020, Accepted July 24, 2020*)

Abstract. In this paper, the bending behavior of single-walled carbon nanotube-reinforced composite (CNTRC) laminated plates is studied using various shear deformation plate theories. Several types of reinforcement material distributions, a uniform distribution (UD) and three functionally graded distributions (FG), are inspected. A generalized higher-order deformation plate theory is utilized to derive the field equations of the CNTRC laminated plates where an analytical technique based on Navier's series is utilized to solve the static problem for simply-supported boundary conditions. A detailed numerical analysis is carried out to examine the influence of carbon nanotube volume fraction, laminated composite structure, side-to-thickness, and aspect ratios on stresses and deflection of the CNTRC laminated plates.

Keywords: bending; carbon nanotube-reinforced composites; laminated plates; generalized higher-order deformation plate theory; simply-supported edge conditions

1. Introduction

Carbon nanotubes, namely CNTs, are known as a novel innovative material with superior thermo-mechanical and electrical properties (Lau *et al*. 2004, Esawi and Farag 2007). Recently, carbon nanotubes were considered as an excellent alternative to classical fiber-reinforced composites, due to their perfect bonding with the polymeric matrix. The CNT-reinforced composite (CNTRC) structures have been applied in numerous engineering applications, such as aerospace, automobile and marine structures, due to their excellent resilience, as well as to their very low density and high strength (100 times greater than steel) (Griebel and Hamaekers 2004, Fidelus and Wiesel 2007, Han Y and Elliott 2007, Zhu *et al* 2007).

To evaluate the performance of CNTRC structures, several numerical simulations have been performed. Shen (2009) performed the bending analysis of a temperature-dependent CNTRC plate by employing the two steps perturbation technique. Shen and Zhang (2010) analyzed buckling and postbuckling of perfect and imperfect FG composite plates reinforced by single-walled carbon nanotubes (SWCNTs), under the effect of a parabolic temperature variation. Wang and Shen (2011) investigated the elastic foundation and temperature effects on the vibration behavior of uniformly distributed UD and functionally graded FG-CNTRC plates, by utilizing the improved perturbation technique. They also investigated the nonlinear dynamic response of single-layer and three-layer CNTRC plates under the same conditions (Wang and Shen 2011). The impact of the material distribution, thermal environments, and pressure loads on the bending response of FG-CNTRC plates was analyzed by Kaci *et al.* (2012). In turn, Zhu *et al.* (2012) applied the finite element method (FEM) and the first order shear deformations plate theory (FSDT) for free vibration and static behaviors of CNTRC plates with different boundary conditions. Using the FSDT and the element free kp-Ritz method, Lei *et al.* (2013a, 2013b, 2013c) examined the nonlinear bending, buckling and free vibration behaviors of single-walled FG-CNTRC plates based on Eshelby-Mori-Tanaka's model with different boundary conditions. Alibeigloo (2013) used a three-dimensional (3D) theory of elasticity to analyze the bending of simply supported CNTRC plates combined with piezoelectric layers. In addition, Alibeigloo and Liew (2013) investigated the bending behavior of simply supported FG-CNTRC rectangular plates subjected to thermo-mechanical loads. Natarajan *et al*. (2014) developed a QUAD-8 shear flexible element, based on higher-order shear deformation plate theory (HSDT), to investigate the bending and the vibration responses of CNTRC sandwich plates. Rafiee *et al*. (2014) studied the nonlinear dynamic stability of perfect and imperfect piezoelectric single-walled FG-CNTRC plates, under thermal and electrical loads,

*Corresponding author, Ph.D.
E-mail: daikh.ahmed.amine@gmail.com

ISSN: 1598-8198 (Print), 1598-818X (Online)

using Galerkin's method associated with the FSDT. The free vibration behavior of CNTRC plates with elastically restrained edges was determined by Zhang *et al*. (2015), using element-free improved moving least-square IMLS-Ritz method. By utilizing HSDT and Isogeometric Analysis IGA, Phung-Van *et al*. (2015) studied static and dynamic responses of CNTRC plates. Moreover, Zhang and Liew (2015) employed the IMLS-Ritz approximation and the FSDT to perform a nonlinear deformation analysis of FG-CNTRC quadrilateral plates. Ansari *et al*. (2015) studied the nonlinear forced vibration responses of CNTRC plates on the basis of the generalized differential quadrature (GDQ) and the FSDT. Wattanasakulpong and Chaikittiratana (2015) presented an exact analytical solution to analyze buckling, bending, and free vibration of CNTRC plates using third order TSDT and sinusoidal SSDT shear deformation plate theories. Kiani (2015) examined natural frequencies of CNTRC plates with piezoelectric face layers by employing the FSDT, Ritz formulation and Chebyshev polynomials. The influence of a rectangular cutout in CNTRC plates on natural frequencies was studied by Mirzaei and Kiani (2016), using the FSDT. Besides, Shams *et al*. (2016) utilized the element-free Galerkin EFG and the FSDT with a modified shear correction factor to analyze FG-CNTRC plate buckling, under the effect of a high temperature. Taghizadeh (2017) analyzed stresses and displacements of CNTRC plates associated with piezoelectric face layers, using the FSDT and the TSDT. Thai *et al*. (2017) carried out an analysis on vibration and bending of CNTRC plates, by employing the mesh free formulations combined with the HSDT. Mehar and Panda (1965) performed an experimental analysis and a numerical simulation to study stress and deflection behaviors of CNTRC plates. The second-order shear deformation theory was employed by Karami *et al*. (2018) to study the size-dependent mechanical response of CNTRC plates in presence of Winkler-Pasternak foundations. The influence of porosity on buckling response of uniform and functionally graded CNTRC plates was examined by Guessas *et al*. (2018), using the FSDT. The cell-based smoothed discrete shear gap method associated with three-node triangular elements CS-DSG3 was utilized by Truong-Thi *et al*. (2018) to study static and vibration behaviors of CNTRC rectangular plates. Trang and Tung (2018) investigated the influence of the tangential edge restraints, compressive and thermo-mechanical loads on buckling and postbuckling of simply supported CNTRC plates, based on the classical plate theory CPT. Fazzolari (2018) studied temperature-dependent stability and vibration of CNTRC plates, using the Quasi-3D plate theory and Ritz method. Bakhadda *et al*. (2018) examined the vibration and the bending behaviors of CNTRC plates, by employing a hyperbolic shear deformation plate theory, while Draoui *et al*. (2019) presented static and dynamic analyses of CNTRC sandwich plates using the FSDT.

Due to the limitations of CBT and FSDT for the analysis of plates, higher order shear deformation theories are developed by considering the transverse shear deformation (Bensattalah *et al*. 2018, Belmahi *et al*. 2019, Batou *et al*. 2019, Salah *et al*. 2019, Bensattalah *et al*. 2019, Boulal *et al*. 2020, Karami *et al*. 2018a, b, Karami *et al*. 2019a, b, Karami *et al*. 2020a, b, Shahsavari *et al*. 2018, Shahsavari *et al*. 2019, Chelahi *et al*. 2020, Daikh *et al*. 2020a).

In the current paper, based on the HSDT, an analytical analysis is conducted to examine the deflection and the stresses of cross-ply simply supported CNTRC laminated plates subjected to a transverse sinusoidal loading. Material properties of carbon nanotubes are supposed to vary in the thickness direction in a functionally graded form. The equilibrium equations are extracted based on the principle of virtual work, and then analytically resolved to provide simply supported supports. The accuracy of the proposed model is verified by comparing the obtained results with those in the literature. Various HSDTs are utilized to examine in detail the influence of volume fraction of carbon nanotubes, laminated composite structure, side-to-thickness, as well as aspect ratios, on axial and shear stresses and transverse deflection of the CNTRC laminated plates.

2. CNTRC laminated plates

Consider a rectangular CNTRC laminated plate of length (a), width (b) and thickness (h), as shown in Fig. 1. Each layer of the considered plate is reinforced by single-walled carbon nanotubes (SWCNTs) according to a uniform distribution (UD) across the thickness or functionally graded distribution (FG). Volume fractions of several reinforcement material distributions types is mathematically expressed as follows (Daikh *et al*. 2020b) (see Fig. 2):

FG-X CNTRC laminated plate

$$V_{cnt} = 2\frac{\left|2|z| - \left|z_{(k-1)} + z_{(k)}\right|\right|}{z_{(k)} - z_{(k-1)}} V_{cnt}^{*} \tag{1}$$

FG-◊ CNTRC laminated plate

$$V_{cnt} = 2\left(1 - \frac{\left|2|z| - \left|z_{(k-1)} + z_{(k)}\right|\right|}{z_{(k)} - z_{(k-1)}}\right) V_{cnt}^{*} \tag{2}$$

FG-V CNTRC laminated plate

$$V_{cnt} = 1 - \left(\frac{2z - z_{(k)} - z_{(k-1)}}{z_{(k)} - z_{(k-1)}}\right) V_{cnt}^{*} \tag{3}$$

UD CNTRC laminated plate

$$V_{cnt} = V_{cnt}^{*} \tag{4}$$

where FG-V CNTRC, FG-◊ CNTRC and FG-X CNTRC indicate the functionally graded distributions, and UD CNTRC indicate the uniform distribution. $z_{(k)}$ and $z_{(k-1)}$ are the vertical positions of the bottom surface and the top surface of the k^{th} layer of the CNTRC laminated plate. It is noted that V_{cnt} is the volume fraction of the carbon nanotubes and V_{cnt}^{*} is a given volume fraction of CNTs, which can be calculate from the following equation

$$V_{cnt}^{*} = \frac{W_{cnt}}{W_{cnt} + (\rho_{cnt}/\rho_{m})(1 - W_{cnt})} \tag{5}$$

where W_{cnt}, ρ_{cnt} and ρ_{m} are the CNTs mass fraction, CNTs mass density and polymer matrix mass density, respectively.

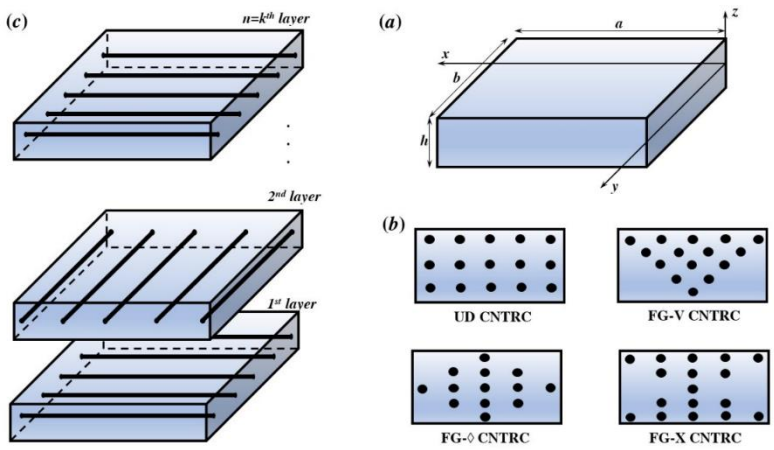

Fig. 1 Geometry and cross-sections of FG-CNTRC Laminated plate

Material properties of the CNTRC laminated plates are made of a mixture of an isotropic polymer matrix and SWCNTs, constructed using the extended rule of mixture. The effective Young's modulus (E) and shear modulus (G) of a CNTRC sheet can be written as

$$\begin{aligned} E_{11}^k &= \eta_1 V_{cnt}^k E_{11}^{cnt} + V_p^k E_p \\ \frac{\eta_2}{E_{22}^k} &= \frac{V_{cnt}^k}{E_{22}^{cnt}} + \frac{V_p^k}{E_p} \\ \frac{\eta_3}{G_{12}^k} &= \frac{V_{cnt}^k}{G_{12}^{cnt}} + \frac{V_p^k}{G_p} \end{aligned} \tag{6}$$

where E_{11}^k; E_{22}^k are the Young's modulus across the plane directions (x, z), and G_{12}^k is the shear modulus of the plate composites. The superscripts p and cnt refer to the properties of the polymer and the SWCNTs, respectively.

The CNT efficiency parameters η_i $(i = 1,2,3)$ are given by:

for $V_{cnt}^* = 0.11$; $\eta_1 = 0.149$,$\eta_2 = \eta_3 = 0.934$.
for $V_{cnt}^* = 0.14$; $\eta_1 = 0.150$,$\eta_2 = \eta_3 = 0.941$.
for $V_{cnt}^* = 0.17$; $\eta_1 = 0.149$,$\eta_2 = \eta_3 = 1.381$.

It is noticed that the sum of the volume fractions of the polymer and CNT constituents equals to unity

$$V_{cnt}^k + V_p^k = 1 \tag{7}$$

Poisson's ratio ν_{12}^k and mass density ρ^k of k layer are expressed as

$$\nu_{12}^k = V_{cnt}^k \nu_{12}^{cnt} + V_p^k \nu_p \tag{8}$$

$$\rho^k = V_{cnt}^k \rho_{cnt} + V_p^k \rho_p \tag{9}$$

3. Theoretical formulation

Consider a rectangular CNTRC laminated plate composed of k^{th} layers, as shown in Fig. 1(c). The displacement components based on the HSDT are given by

$$\begin{aligned} u(x,y,z) &= u_0 - z\frac{\partial w_0}{\partial x} + f(z)\varphi_1 \\ v(x,y,z) &= v_0 - z\frac{\partial w_0}{\partial y} + f(z)\varphi_2 \\ w(x,y,z) &= w_0 \end{aligned} \tag{10}$$

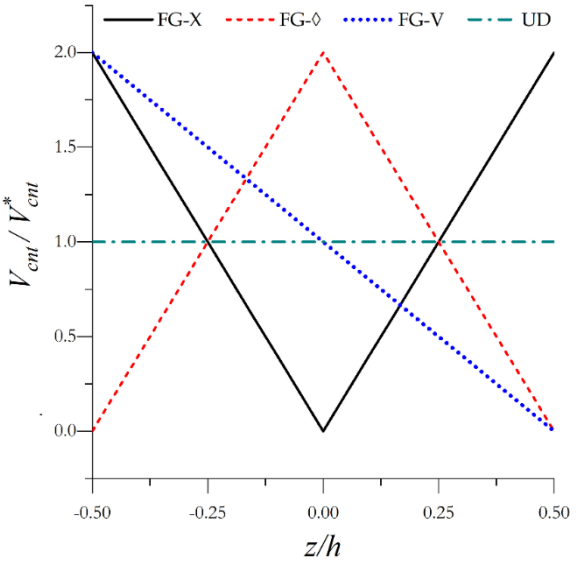

Fig. 2 Variation of CNTs volume fraction through the CNTRC plate thickness

where u_0, v_0, and w_0, are the displacement components along the x, y and z directions, respectively, φ_1 and φ_2 rotations of the transverse normal around the x and y axes, respectively. The shape function $f(z)$ determining the distribution of the transverse shear strains and stresses along the thickness of the CNTRC laminated plate is given by the following forms:

For the FSDT

$$f(z) = z \tag{11}$$

For the TSDT of Reddy (1984)

$$f(z) = z\left(1 - \frac{4z^2}{3h^2}\right) \tag{12}$$

For the SSDT of Touratier (1991)

$$f(z) = \frac{h}{\pi}\sin\left(\frac{z}{h}\right) \tag{13}$$

For the ESDT of Karama *et al.* (2009)

$$f(z) = ze^{-2\left(\frac{z}{h}\right)^2} \tag{14}$$

For the HSDT of Daikh and Zenkour (2019a, b)

$$f(z) = z\left(1 - \frac{3z^2}{2h^2} + \frac{2z^4}{5h^4}\right) \tag{15}$$

The used higher-order shear deformation theories accounts for the distribution of transvers shear stresses that satisfies the free transverse shear stresses condition on the upper and lower surfaces of the sandwich plate.

The deformation components associated with the above displacements can be expressed as

$$\begin{Bmatrix}\varepsilon_{xx}\\ \varepsilon_{yy}\\ \gamma_{xy}\end{Bmatrix} = \begin{Bmatrix}\varepsilon^0_{xx}\\ \varepsilon^0_{yy}\\ \gamma^0_{xy}\end{Bmatrix} + z\begin{Bmatrix}\varepsilon^1_{xx}\\ \varepsilon^1_{yy}\\ \gamma^1_{xy}\end{Bmatrix} + f(z)\begin{Bmatrix}\varepsilon^2_{xx}\\ \varepsilon^2_{yy}\\ \gamma^2_{xy}\end{Bmatrix},$$
$$\varepsilon_{zz} = 0, \quad \begin{Bmatrix}\gamma_{yz}\\ \gamma_{xz}\end{Bmatrix} = \frac{\mathrm{d}f(z)}{\mathrm{d}z}\begin{Bmatrix}\gamma^0_{yz}\\ \gamma^0_{xz}\end{Bmatrix}, \tag{16}$$

where

$$\begin{Bmatrix}\varepsilon^0_{xx}\\ \varepsilon^0_{yy}\\ \gamma^0_{xy}\end{Bmatrix} = \begin{Bmatrix}\frac{\partial u_0}{\partial x}\\ \frac{\partial v_0}{\partial y}\\ \frac{\partial v_0}{\partial x} + \frac{\partial u_0}{\partial y}\end{Bmatrix}, \quad \begin{Bmatrix}\varepsilon^1_{xx}\\ \varepsilon^1_{yy}\\ \gamma^1_{xy}\end{Bmatrix} = -\begin{Bmatrix}\frac{\partial^2 w_0}{\partial x^2}\\ \frac{\partial^2 w_0}{\partial y^2}\\ 2\frac{\partial^2 w_0}{\partial x \partial y}\end{Bmatrix},$$
$$\begin{Bmatrix}\varepsilon^2_{xx}\\ \varepsilon^2_{yy}\\ \gamma^2_{xy}\end{Bmatrix} = \begin{Bmatrix}\frac{\partial \varphi_1}{\partial x}\\ \frac{\partial \varphi_2}{\partial y}\\ \frac{\partial \varphi_2}{\partial x} + \frac{\partial \varphi_1}{\partial y}\end{Bmatrix}, \quad \begin{Bmatrix}\gamma^0_{yz}\\ \gamma^0_{xz}\end{Bmatrix} = \begin{Bmatrix}\varphi_x\\ \varphi_y\end{Bmatrix}. \tag{17}$$

Since the CNTRC laminate is made of k^{th} layers, the constitutive stress-strain relations are stated as

$$\begin{Bmatrix}\sigma_{xx}\\ \sigma_{yy}\\ \tau_{yz}\\ \tau_{xz}\\ \tau_{xy}\end{Bmatrix}^{(k)} = \begin{bmatrix}\bar{Q}^k_{11} & \bar{Q}^k_{12} & 0 & 0 & 0\\ \bar{Q}^k_{12} & \bar{Q}^k_{22} & 0 & 0 & 0\\ 0 & 0 & \bar{Q}^k_{44} & 0 & 0\\ 0 & 0 & 0 & \bar{Q}^k_{55} & 0\\ 0 & 0 & 0 & 0 & \bar{Q}^k_{66}\end{bmatrix}\begin{Bmatrix}\varepsilon_{xx}\\ \varepsilon_{yy}\\ \gamma_{yz}\\ \gamma_{xz}\\ \gamma_{xy}\end{Bmatrix}^{(k)} \tag{18}$$

where the transformed material constants $\bar{Q}^k_{ij}$ are expressed as

$$\begin{aligned}\bar{Q}^k_{11} &= Q_{11}cos^4\theta_k + 2(Q_{12} + 2Q_{66})sin^2\theta_k cos^2\theta_k + Q_{22}sin^4\theta_k\\ \bar{Q}^k_{12} &= (Q_{11} + Q_{22} - 4Q_{66})sin^2\theta_k cos^2\theta_k + Q_{12}(sin^4\theta_k + cos^4\theta_k)\\ \bar{Q}^k_{22} &= Q_{11}sin^4\theta_k + 2(Q_{12} + 2Q_{66})sin^2\theta_k cos^2\theta_k + Q_{22}cos^4\theta_k\\ \bar{Q}^k_{66} &= (Q_{11} + Q_{22} - 2Q_{12} - 2Q_{66})sin^2\theta_k cos^2\theta_k + Q_{66}(sin^4\theta_k + cos^4\theta_k)\\ \bar{Q}^k_{44} &= Q_{44}cos^2\theta_k + Q_{55}sin^2\theta_k\\ \bar{Q}^k_{55} &= Q_{55}cos^2\theta_k + Q_{44}sin^2\theta_k\end{aligned} \tag{19}$$

where θ_k is the lamination angle of the k^{th} layer, and

$$Q_{11} = \frac{E_{11}}{1 - \nu_{12}\nu_{21}}, Q_{22} = \frac{E_{22}}{1 - \nu_{12}\nu_{21}}, Q_{12} = \frac{\nu_{12}E_{22}}{1 - \nu_{12}\nu_{21}}$$
$$Q_{44} = G_{23}, Q_{55} = G_{13}, Q_{66} = G_{12} \tag{20}$$

The strain energy of the CNTRC laminated plate is given as

$$\delta U = \int_V [\sigma^k_{xx}\delta\varepsilon_{xx} + \sigma^k_{yy}\delta\varepsilon_{yy} + \tau^k_{xy}\delta\gamma_{xy} + \tau^k_{yz}\delta\gamma_{yz} + \tau^k_{xz}\delta\gamma_{xz}]dV \tag{21}$$

In addition, the potential energy due to the transverse applied loading is

$$\delta V = \int_A q\delta w \mathrm{d}A \tag{22}$$

Based on the principle of virtual work, the equilibrium equations are derived as follows

$$\begin{aligned}\frac{\partial N_{xx}}{\partial x} + \frac{\partial N_{xy}}{\partial y} &= 0\\ \frac{\partial N_{xy}}{\partial x} + \frac{\partial N_{yy}}{\partial y} &= 0\\ \frac{\partial^2 M_{xx}}{\partial x^2} + 2\frac{\partial^2 M_{xy}}{\partial x \partial y} + \frac{\partial^2 M_{yy}}{\partial y^2} + q &= 0\\ \frac{\partial P_{xx}}{\partial x} + \frac{\partial P_{xy}}{\partial y} - R_{xz} &= 0\\ \frac{\partial P_{xy}}{\partial x} + \frac{\partial P_{yy}}{\partial y} - R_{yz} &= 0,\end{aligned} \tag{23}$$

Note that (N_{xx}, N_{yy}, N_{xy}) indicate the total in-plane force resultants, (M_{xx}, M_{yy}, M_{xy}) are the stress couples, (P_{xx}, P_{yy}, P_{xy}) and (R_{yz}, R_{xz}) are the additional stress couples and transverse shear stress resultants, respectively, and they are expressed as

$$\begin{Bmatrix}N_{xx}\\ N_{yy}\\ N_{xy}\end{Bmatrix} = \sum_{k=1}^{n}\int_{z_{(k-1)}}^{z_{(k)}}\begin{Bmatrix}\sigma_{xx}\\ \sigma_{yy}\\ \tau_{xy}\end{Bmatrix}^k \mathrm{d}z \tag{24}$$

$$\begin{Bmatrix}M_{xx}\\ M_{yy}\\ M_{xy}\end{Bmatrix} = \sum_{k=1}^{n}\int_{z_{(k-1)}}^{z_{(k)}}\begin{Bmatrix}\sigma_{xx}\\ \sigma_{yy}\\ \tau_{xy}\end{Bmatrix}^k z\mathrm{d}z \tag{25}$$

$$\begin{Bmatrix}P_{xx}\\ P_{yy}\\ P_{xy}\end{Bmatrix} = \sum_{k=1}^{n}\int_{z_{(k-1)}}^{z_{(k)}}\begin{Bmatrix}\sigma_{xx}\\ \sigma_{yy}\\ \tau_{xy}\end{Bmatrix}^k f(z)\mathrm{d}z \tag{26}$$

$$\begin{Bmatrix}R_{yz}\\ R_{xz}\end{Bmatrix} = \sum_{k=1}^{n}\int_{z_{(k-1)}}^{z_{(k)}}\begin{Bmatrix}\tau_{yz}\\ \tau_{xz}\end{Bmatrix}^k \frac{\mathrm{d}f(z)}{\mathrm{d}z}\mathrm{d}z \tag{27}$$

The stress resultants of the CNTRC laminated plate are given by

$$\begin{Bmatrix}\{N\}\\ \{M\}\\ \{P\}\end{Bmatrix} = \begin{bmatrix}[A] & [B] & [C]\\ [B] & [D] & [F]\\ [C] & [F] & [H]\end{bmatrix}\begin{Bmatrix}\{\varepsilon^0\}\\ \{\varepsilon^1\}\\ \{\varepsilon^2\}\end{Bmatrix}$$
$$\begin{Bmatrix}R_{yz}\\ R_{xz}\end{Bmatrix} = \begin{bmatrix}J_{44} & 0\\ 0 & J_{55}\end{bmatrix}\begin{Bmatrix}\gamma^0_{yz}\\ \gamma^0_{xz}\end{Bmatrix} \tag{28}$$

where

$$\{N\} = \{N_{xx} \quad N_{yy} \quad N_{xy}\}^T, \{M\} = \{M_{xx} \quad M_{yy} \quad M_{xy}\}^T,$$
$$\{P\} = \{P_{xx} \quad P_{yy} \quad P_{xy}\}^T, \{\varepsilon^0\} = \{\varepsilon^0_{xx} \quad \varepsilon^0_{yy} \quad \gamma^0_{xy}\}^T, \tag{29}$$
$$\{\varepsilon^1\} = \{\varepsilon^1_{xx} \quad \varepsilon^1_{yy} \quad \gamma^1_{xy}\}^T, \{\varepsilon^2\} = \{\varepsilon^2_{xx} \quad \varepsilon^2_{yy} \quad \gamma^2_{xy}\}^T.$$

Here A_{ij}, B_{ij},..., H_{ij} are the composite plate stiffness, given by

$$\{A_{ij}, B_{ij}, D_{ij}, C_{ij}, F_{ij}, H_{ij}\} = \sum_{k=1}^{n} \int_{z_{(k-1)}}^{z_{(k)}} \bar{Q}_{ij}^{k} \{1, z, z^2, f(z), zf(z), f(z)^2\} \mathrm{d}z, \quad (30)$$

$$J_{cc} = \bar{K} \sum_{k=1}^{n} \int_{z_{(k-1)}}^{z_{(k)}} Q_{cc}^{k} \left[\frac{\mathrm{d}f(z)}{\mathrm{d}z}\right]^2 \mathrm{d}z, (i, j = 1,2,6, c = 4,5)$$

where $\bar{K} = 5/6$ denote the FSDT shear correction factor.

4. Analytical solutions

The current analysis focuses on cross-ply CNTRC laminated plate subjected to simply-supported edge conditions. These conditions are given by:

$$\begin{aligned} v_0^1 = w_0^1 = \varphi_2^1 = N_{xx}^1 = M_{xx}^1 = P_{xx}^1 = 0 \quad \text{at} \quad x = 0, a, \\ u_0^1 = w_0^1 = \varphi_1^1 = N_{yy}^1 = M_{yy}^1 = P_{yy}^1 = 0 \quad \text{at} \quad y = 0, b. \end{aligned} \quad (31)$$

Navier solution is applied to obtain the closed form solutions that satisfy the above boundary conditions of the present plate can be written as follows

$$\begin{aligned} \{u_0, \varphi_x\} &= \sum_{m=1}^{\infty} \sum_{n=1}^{\infty} \{U_{mn}, X_{mn}\} \cos(\lambda x) \sin(\beta y) \\ \{v_0, \varphi_y\} &= \sum_{m=1}^{\infty} \sum_{n=1}^{\infty} \{V_{mn}, Y_{mn}\} \sin(\lambda x) \cos(\beta y) \\ \{w_0, q\} &= \sum_{m=1}^{\infty} \sum_{n=1}^{\infty} \{W_{mn}, q_0\} \sin(\lambda x) \sin(\beta y) \end{aligned} \quad (32)$$

where $\lambda = m\pi/a$, $\mu = n\pi/b$, and U_{mn}, X_{mn}, V_{mn}, Y_{mn} and W_{mn} are unknown arbitrary parameters. q_0 is the intensity of the transverse load applied at the composite plate center. By substituting Eq. (32) into Eq. (23), the following formulation can be obtained

$$[L]\{\Lambda\} = \{F\} \quad (33)$$

The columns $\{\Lambda\}$ and $\{F\}$, as well as the elements L_{ij} of the symmetric matrix (L) are expressed as

$$\{\Lambda\} = \{U, V, W, X, Y\}^T \quad (34)$$

$$\{F\} = \{0, 0, -q_0, 0, 0\}^T \quad (35)$$

$$\begin{aligned} L_{11} &= A_{11}\lambda^2 + A_{66}\mu^2 \\ L_{12} &= \lambda\mu(A_{12} + A_{66}) \\ L_{13} &= -B_{11}\lambda^3 - \lambda\mu^2(B_{12} + 2B_{66}) \\ L_{14} &= C_{11}\lambda^2 + C_{66}\mu^2 \\ L_{15} &= \lambda\mu(C_{12} + C_{66}) \\ L_{22} &= A_{66}\lambda^2 + A_{22}\mu^2 \\ L_{23} &= -B_{22}\mu^3 - \mu\lambda^2(B_{12} + 2B_{66}) \\ L_{24} &= L_{15} \\ L_{25} &= C_{66}\lambda^2 + C_{22}\mu^2 \\ L_{33} &= D_{11}\lambda^4 + (2D_{12} + 4D_{66})\lambda^2\mu^2 + D_{22}\mu^4 \\ L_{34} &= -F_{11}\lambda^3 - \lambda\mu^2(F_{12} + 2F_{66}) \\ L_{35} &= -F_{22}\mu^3 - \mu\lambda^2(F_{12} + 2F_{66}) \\ L_{44} &= J_{44} + H_{11}\lambda^2 + H_{66}\mu^2 \\ L_{45} &= \lambda\mu(H_{12} + H_{66}) \\ L_{55} &= J_{55} + H_{66}\lambda^2 + H_{22}\mu^2 \end{aligned} \quad (36)$$

The axial and shear stresses in terms of Young's modulus and the parameters U_{mn}, X_{mn}, V_{mn}, Y_{mn} and W_{mn} can be written as

$$\begin{aligned} \sigma_{xx}^k = \sum_{m,n=1,3,5,\ldots}^{\infty} [&- Q_{11}^k(\lambda U_{mn} - \boldsymbol{z}\lambda^2 W_{mn} + \boldsymbol{f}(\boldsymbol{z})\lambda X_{mn}) \\ &- Q_{12}^k(\mu V_{mn} - z\mu^2 W_{mn} + f(z)\mu Y_{mn})] sin(\lambda x) sin(\mu y) \end{aligned} \quad (37)$$

$$\begin{aligned} \sigma_{yy}^k = \sum_{m,n=1,3,5,\ldots}^{\infty} [&- Q_{12}^k(\lambda U_{mn} - z\lambda^2 W_{mn} + f(z)\lambda X_{mn}) \\ &- Q_{22}^k(\mu V_{mn} - z\mu^2 W_{mn} + f(z)\mu Y_{mn})] \, sin(\lambda x) sin(\mu y) \end{aligned} \quad (38)$$

$$\tau_{yz}^k = \sum_{m,n=1,3,5,\ldots}^{\infty} Q_{44}^k g(z)\lambda Y_{mn} sin(\lambda x) cos(\mu y) \quad (39)$$

$$\tau_{xz}^k = \sum_{m,n=1,3,5,\ldots}^{\infty} Q_{55}^k g(z)\lambda X_{mn} cos(\lambda x) sin(\mu y) \quad (40)$$

$$\begin{aligned} \tau_{xy}^k = \sum_{m,n=1,3,5,\ldots}^{\infty} [&Q_{66}^k \, \lambda U_{mn} + \mu V_{mn} - 2z\lambda\mu W_{mn} \\ &+ f(z)(\lambda X_{mn} + \mu Y_{mn})]) \, cos(\lambda x) cos(\mu y) \end{aligned} \quad (41)$$

5. Numerical results

During the current analysis, PmPV (Polymer) was used as the matrix and the armchair (10,10) SWCNTs to reinforce the polymeric matrix.

The effective wall thickness acquired for (10,10) SWCNT which satisfies the Vodenitcharova -Zhang criterion (Vodenitcharova and Zhang 2003) is $h = 0.067$ nm with radius $R = 0.68$ nm and length $L = 9.26$ nm. The elastic material characteristics of the two constituents are:

$$\nu^p = 0.34; \ \rho^p = 1150\text{kg/m}^3; \ E^p = 2.1\text{GPa}.$$
$$\nu_{12}^{cnt} = 0.175; \ \rho^{cnt} = 1400\text{kg/m}^3; \ E_{11}^{cnt} = 5.6466 \text{ Tpa};$$
$$E_{22}^{cnt} = 7.0800 \text{ Tpa}.$$
$$G_{12}^{cnt} = G_{13}^{cnt} = G_{23}^{cnt} = 1.9445\text{Tpa}.$$

The normalized transverse displacement and normalized stresses are presented with the following non-dimensionality forms

$$\bar{w} = \frac{10^3 D_0}{a^4 q_0} w\left(\frac{a}{2}, \frac{b}{2}\right) \quad (42)$$

$$\bar{\sigma}_{xx} = -\frac{h^2}{a^2 q_0} \sigma_{xx}\left(\frac{a}{2}, \frac{b}{2}, \frac{h}{2}\right) \quad (43)$$

$$\bar{\sigma}_{yy} = -\frac{h^2}{a^2 q_0} \sigma_{yy}\left(\frac{a}{2}, \frac{b}{2}, \frac{h}{2}\right) \quad (44)$$

$$\bar{\tau}_{xy} = \frac{h^2}{a^2 q_0} \tau_{xy}\left(0, 0, -\frac{h}{2}\right) \quad (45)$$

$$\bar{\tau}_{xz} = \frac{h^2}{a^2 q_0} \tau_{xz}\left(0, \frac{b}{2}, 0\right) \quad (46)$$

where

$$D_0 = \frac{E_p h^3}{12\left[1 - \left(\nu_p\right)^2\right]} \quad (47)$$

In order to confirm the validity of the used HSDT (41), nondimensional center deflection and stresses of the laminated composite are established in Table 1. The used material properties are:

$$E_1 = 25E_2; \ G_{12} = G_{13} = 0.5E_2; \ G_{23} = 0.2E_2;$$
$$\nu_{12} = 0.25.$$

Table 1 Nondimensional* deflection and stresses in four-layer (0°/90°/90°/0°) square laminated composite (*a/h*=4)

Source	$\widetilde{w}$	$\tilde{\sigma}_{xx}$	$\tilde{\sigma}_{yy}$	$\tilde{\tau}_{yz}$	$\tilde{\tau}_{xy}$	$\tilde{\tau}_{xz}$
HSDT	1.9026	0.6752	0.6338	0.2430	0.0446	0.2118
TSDT (37)	1.8937	0.6651	0.6322	0.2389	0.0440	0.2064
SSDT (38)	1.9088	0.6830	0.6349	0.2462	0.0450	0.2162
ESDT (38)	1.9193	0.7004	0.6367	0.2532	0.0459	0.2264
FSDT (37)	1.7100	0.4059	0.5765	0.1963	0.0308	0.1398

*$\widetilde{w} = 10^2\left(\frac{h^3 E_2}{q_0 a^4}\right) w\left(\frac{a}{2},\frac{b}{2}\right)$, $\tilde{\sigma}_{xx} = -\frac{h^2}{a^2 q_0}\sigma_{xx}\left(\frac{a}{2},\frac{b}{2},\frac{h}{2}\right)$, $\tilde{\sigma}_{yy} = -\frac{h^2}{a^2 q_0}\sigma_{yy}\left(\frac{a}{2},\frac{b}{2},\frac{h}{4}\right)$, $\tilde{\tau}_{yz} = \frac{h}{a q_0}\tau_{yz}\left(\frac{a}{2},0,0\right)$, $\tilde{\tau}_{xz} = \frac{h}{a q_0}\tau_{xz}\left(0,\frac{b}{2},0\right)$, , $\tilde{\tau}_{xy} = \frac{h^2}{a^2 q_0}\tau_{xy}\left(0,0,-\frac{h}{2}\right)$.

according to Table 1, the proposed HSDT is in a good agreement with those generated by Reddy (38) and Karama *et al*. (40), which indicate the precision and correctness of the proposed formulation.

To analyze the effect of carbon nanotube distribution, four laminated composite plates are presented; a single layer [0°] CNTRC plate, an asymmetric two layered [0°/90°] CNTRC laminated plate, and a symmetric three and four layered [0°/90°/0°] and [0°/90°/90°/0°] CNTRC laminated plates. The CNTRC plates are subjected to a transversely sinusoidal loading $q_0 = 1e5\ \mathrm{N/m^2}$.

Nondimensional center deflection of a single layer (0°) and CNTRC laminated plate is illustrated in Table 2 for

Table 2 Nondimensional center deflection of single layer and laminated CNTRC plate (*a/h*=10, *a/b*=1)

	Source	$V^*_{cnt}=0.11$				$V^*_{cnt}=0.14$				$V^*_{cnt}=0.17$			
		UD	FG-X	FG-◊	FG-V	UD	FG-X	FG-◊	FG-V	UD	FG-X	FG-◊	FG-V
SL (0°)	HSDT	0.4959	0.4218	0.7094	0.5864	0.4391	0.3810	0.6163	0.5130	0.3173	0.2720	0.4533	0.3766
	TSDT (24)	0.4964	0.4227	0.7081	0.5869	0.4396	0.3817	0.6148	0.5133	0.3177	0.2723	0.4526	0.3769
	SSDT (24)	0.4953	0.4208	0.7104	0.5859	0.4383	0.3800	0.6168	0.5121	0.3170	0.2715	0.4537	0.3763
	FSDT	0.4575	0.3856	0.6457	0.5488	0.4026	0.3433	0.5569	0.4766	0.2931	0.2441	0.4177	0.3523
(0°/90°)	HSDT	0.8294	0.6439	1.1981	0.9199	0.7037	0.5412	1.0415	0.7876	0.5339	0.4124	0.7697	0.5908
	TSDT	0.8311	0.6459	1.1993	0.9216	0.7055	0.5432	1.0428	0.7893	0.5350	0.4137	0.7703	0.5918
	SSDT	0.8280	0.6422	1.1970	0.9184	0.7023	0.5394	1.0405	0.7861	0.5330	0.4113	0.7691	0.5899
	FSDT	0.8302	0.6498	1.1876	0.9213	0.7062	0.5480	1.0333	0.7903	0.5342	0.4159	0.7625	0.5907
(0°/90°/0°)	HSDT	0.4719	0.4384	0.5088	0.4816	0.4142	0.3823	0.4482	0.4226	0.3024	0.2796	0.3244	0.3078
	TSDT	0.4725	0.4394	0.5087	0.4819	0.4148	0.3833	0.4482	0.4229	0.3027	0.2802	0.3244	0.3079
	SSDT	0.4712	0.4374	0.5086	0.4812	0.4135	0.3813	0.4480	0.4222	0.3020	0.2789	0.3244	0.3075
	FSDT	0.4395	0.4203	0.4585	0.4449	0.3835	0.3656	0.3999	0.3875	0.2819	0.2683	0.2929	0.2845
(0°/90°/90°/0)	HSDT	0.4333	0.4154	0.4506	0.4459	0.3759	0.3589	0.3911	0.3868	0.2781	0.2655	0.2881	0.2853
	TSDT	0.4338	0.4161	0.4510	0.4465	0.3764	0.3596	0.3914	0.3873	0.2785	0.2659	0.2883	0.2856
	SSDT	0.4327	0.4148	0.4501	0.4454	0.3754	0.3583	0.3907	0.3862	0.2778	0.2651	0.2878	0.2849
	FSDT	0.4077	0.3968	0.4174	0.4191	0.3514	0.3413	0.3593	0.3612	0.2620	0.2539	0.2672	0.2685

Table 3 Nondimensional stresses of single layer [0°] CNTRC plate (*a/h*=10, *a/b*=1)

	Source	$V^*_{cnt}=0.11$				$V^*_{cnt}=0.14$				$V^*_{cnt}=0.17$			
		$\bar{\sigma}_{xx}$	$\bar{\sigma}_{yy}$	$\bar{\tau}_{xy}$	$\bar{\tau}_{xz}$	$\bar{\sigma}_{xx}$	$\bar{\sigma}_{yy}$	$\bar{\tau}_{xy}$	$\bar{\tau}_{xz}$	$\bar{\sigma}_{xx}$	$\bar{\sigma}_{yy}$	$\bar{\tau}_{xy}$	$\bar{\tau}_{xz}$
UD	HSDT	0.6578	0.0312	0.0154	0.0443	0.6886	0.0282	0.0139	0.0445	0.6531	0.0316	0.0157	0.0443
	TSDT	0.6541	0.0312	0.0154	0.0436	0.6841	0.0282	0.0139	0.0439	0.6496	0.0316	0.0157	0.0436
	SSDT	0.6606	0.0312	0.0155	0.0449	0.6920	0.0282	0.0139	0.0451	0.6559	0.0316	0.0158	0.0449
	FSDT	0.5520	0.0284	0.0138	0.0296	0.5581	0.0254	0.0122	0.0299	0.5511	0.0287	0.0141	0.0296
FG-X	HSDT	0.9208	0.0292	0.0141	0.0404	0.9700	0.0282	0.0135	0.0395	0.9156	0.0326	0.0158	0.0385
	TSDT	0.9155	0.0292	0.0141	0.0397	0.9634	0.0282	0.0135	0.0389	0.9101	0.0326	0.0158	0.0378
	SSDT	0.9249	0.0292	0.0141	0.0409	0.9750	0.0281	0.0135	0.0400	0.9197	0.0326	0.0158	0.0390
	FSDT	0.7416	0.0263	0.0124	0.0265	0.7475	0.0250	0.0116	0.0256	0.7394	0.0289	0.0138	0.0244
FG-◊	HSDT	0.0415	0.0467	0.0214	0.0504	0.0350	0.0403	0.0184	0.0526	0.0327	0.0471	0.0205	0.0536
	TSDT	0.0413	0.0465	0.0214	0.0494	0.0348	0.0401	0.0184	0.0516	0.0326	0.0470	0.0204	0.0526
	SSDT	0.0417	0.0468	0.0215	0.0511	0.0351	0.0403	0.0185	0.0533	0.0328	0.0472	0.0205	0.0543
	FSDT	0.0367	0.0420	0.0191	0.0325	0.0303	0.0359	0.0162	0.0344	0.0293	0.0429	0.0185	0.0356
FG-V	HSDT	1.2454	0.0421	0.0185	0.0434	1.3163	0.0388	0.0160	0.0437	1.2420	0.0456	0.0180	0.0431
	TSDT	1.2383	0.0421	0.0185	0.0427	1.3077	0.0388	0.0160	0.0430	1.2351	0.0456	0.0180	0.0425
	SSDT	1.2508	0.0421	0.0185	0.0440	1.3230	0.0388	0.0161	0.0442	1.2473	0.0457	0.0180	0.0437
	FSDT	1.0413	0.0391	0.0170	0.0289	1.0635	0.0356	0.0146	0.0291	1.0454	0.0424	0.0166	0.0286

Table 4 Nondimensional* stresses of two-ply CNTRC laminated plate [0°/90°] (*a/h*=10, *a/b*=1)

	Source	$V_{cnt}^{*}=0.11$				$V_{cnt}^{*}=0.14$				$V_{cnt}^{*}=0.17$			
		$\bar{\sigma}_{xx}$	$\bar{\sigma}_{yy}$	$\bar{\tau}_{xy}$	$\bar{\tau}_{xz}$	$\bar{\sigma}_{xx}$	$\bar{\sigma}_{yy}$	$\bar{\tau}_{xy}$	$\bar{\tau}_{xz}$	$\bar{\sigma}_{xx}$	$\bar{\sigma}_{yy}$	$\bar{\tau}_{xy}$	$\bar{\tau}_{xz}$
UD	HSDT	0.7838	0.9277	0.0295	0.0221	0.8327	0.9809	0.0256	0.0219	0.7752	0.9188	0.0302	0.0221
	TSDT	0.7850	0.9266	0.0295	0.0218	0.8342	0.9797	0.0256	0.0217	0.7764	0.9177	0.0302	0.0218
	SSDT	0.7828	0.9284	0.0295	0.0222	0.8315	0.9817	0.0256	0.0220	0.7743	0.9195	0.0302	0.0223
	FSDT	0.8036	0.8808	0.0291	0.0159	0.8581	0.9251	0.0252	0.0159	0.7943	0.8732	0.0297	0.0159
FG-X	HSDT	1.1599	1.3539	0.0251	0.0245	1.2131	1.4147	0.0224	0.0254	1.1474	1.3425	0.0282	0.0268
	TSDT	1.1616	1.3529	0.0251	0.0243	1.2152	1.4137	0.0225	0.0252	1.1490	1.3416	0.0282	0.0266
	SSDT	1.1586	1.3546	0.0251	0.0247	1.2114	1.4154	0.0224	0.0255	1.1462	1.3431	0.0282	0.0270
	FSDT	1.1882	1.2861	0.0247	0.0181	1.2494	1.3341	0.0221	0.0188	1.1744	1.2772	0.0278	0.0197
FG-◊	HSDT	0.0203	0.0635	0.0396	0.0204	0.0175	0.0549	0.0343	0.0195	0.0108	0.0532	0.0377	0.0189
	TSDT	0.0203	0.0635	0.0396	0.0201	0.0175	0.0549	0.0343	0.0193	0.0108	0.0531	0.0377	0.0187
	SSDT	0.0203	0.0636	0.0396	0.0207	0.0174	0.0549	0.0343	0.0197	0.0108	0.0532	0.0377	0.0192
	FSDT	0.0207	0.0618	0.0389	0.0141	0.0178	0.0533	0.0337	0.0136	0.0110	0.0519	0.0371	0.0130
FG-V	HSDT	0.0239	0.6135	0.0334	0.0184	0.0204	0.6507	0.0306	0.0173	0.0145	0.6018	0.0375	0.0172
	TSDT	0.0239	0.6130	0.0334	0.0183	0.0204	0.6501	0.0306	0.0172	0.0145	0.6013	0.0375	0.0170
	SSDT	0.0239	0.6139	0.0334	0.0185	0.0204	0.6512	0.0306	0.0174	0.0145	0.6022	0.0375	0.0173
	FSDT	0.0240	0.5911	0.0331	0.0138	0.0205	0.6241	0.0303	0.0131	0.0145	0.5800	0.0371	0.0127

* Same nondimensionalization as used in Table 3, except $\bar{\sigma}_{xx}$ is evaluated at $(x, y, z) = (a/2, b/2, 0)$.

Table 5 Nondimensional* stresses of three-layer CNTRC laminates [0°/90°/0°] (*a/h*=10, *a/b*=1)

	Source	$V_{cnt}^{*}=0.11$				$V_{cnt}^{*}=0.14$				$V_{cnt}^{*}=0.17$			
		$\bar{\sigma}_{xx}$	$\bar{\sigma}_{yy}$	$\bar{\tau}_{xy}$	$\bar{\tau}_{xz}$	$\bar{\sigma}_{xx}$	$\bar{\sigma}_{yy}$	$\bar{\tau}_{xy}$	$\bar{\tau}_{xz}$	$\bar{\sigma}_{xx}$	$\bar{\sigma}_{yy}$	$\bar{\tau}_{xy}$	$\bar{\tau}_{xz}$
UD	HSDT	0.6334	0.3328	0.0144	0.0415	0.6571	0.3676	0.0128	0.0415	0.6298	0.3276	0.0147	0.0415
	TSDT	0.6302	0.3340	0.0144	0.0409	0.6533	0.3691	0.0128	0.0408	0.6267	0.3287	0.0147	0.0409
	SSDT	0.6359	0.3317	0.0144	0.0421	0.6601	0.3662	0.0128	0.0420	0.6322	0.3265	0.0147	0.0421
	FSDT	0.5396	0.3236	0.0130	0.0279	0.5421	0.3572	0.0114	0.0280	0.5391	0.3186	0.0133	0.0279
FG-X	HSDT	1.1427	0.5936	0.0150	0.0349	1.1793	0.6499	0.0138	0.0334	1.1397	0.5845	0.0169	0.0322
	TSDT	1.1376	0.5967	0.0150	0.0344	1.1732	0.6539	0.0138	0.0329	1.1349	0.5876	0.0169	0.0318
	SSDT	1.1466	0.5909	0.0150	0.0353	1.1839	0.6465	0.0138	0.0338	1.1435	0.5819	0.0169	0.0326
	FSDT	0.9981	0.6006	0.0140	0.0241	1.0032	0.6607	0.0128	0.0232	1.0010	0.5912	0.0157	0.0223
FG-◊	HSDT	0.0260	0.0103	0.0141	0.0501	0.0220	0.0089	0.0122	0.0524	0.0207	0.0074	0.0134	0.0548
	TSDT	0.0259	0.0104	0.0140	0.0493	0.0219	0.0089	0.0121	0.0515	0.0206	0.0074	0.0133	0.0538
	SSDT	0.0261	0.0103	0.0141	0.0508	0.0220	0.0089	0.0122	0.0532	0.0207	0.0074	0.0134	0.0555
	FSDT	0.0222	0.0100	0.0123	0.0325	0.0183	0.0086	0.0104	0.0341	0.0179	0.0073	0.0117	0.0355
FG-V	HSDT	0.0267	0.2008	0.0156	0.0419	0.0225	0.2216	0.0145	0.0418	0.0212	0.1962	0.0175	0.0417
	TSDT	0.0266	0.2014	0.0156	0.0412	0.0223	0.2224	0.0144	0.0411	0.0211	0.1968	0.0175	0.0410
	SSDT	0.0268	0.2003	0.0156	0.0425	0.0225	0.2209	0.0145	0.0424	0.0212	0.1957	0.0175	0.0423
	FSDT	0.0231	0.1938	0.0141	0.0279	0.0190	0.2132	0.0129	0.0279	0.0186	0.1893	0.0158	0.0277

* Same nondimensionalization as used in Table 3, except $\bar{\sigma}_{vv}$ is evaluated at $(x, y, z) = (a/2, b/2, h/6)$.

different volume fractions of CNTs ($V_{cnt}^{*} = 0.11, 0.14$ and 0.17) and various reinforcement material distributions. All layers are supposed to be made of the same material and the same thickness. The obtained results of a single layer CNTRC plate are compared with the data provided by Wattanasakulpong and Chaikittiratana (2013).

One can see again that the results are very close each other, which shows the precision of the currently proposed model. Moreover, it is noted that the central deflection decreases with the increase in the CNT volume fraction, because the increase of the latter improves the flexural stiffness of the plate. Besides, for different patterns of the CNTs, the central deflections are maximum for FG-◊ CNTRC plates and are minimum for FG-X CNTRC plates.

Tables 3 depicts nondimensional stresses of a single layer [0°] CNTRC square plate for various reinforcement material distributions, with a side to thickness ratio $a/h = 10$. Tables 4, 5 and 6 correspond to antisymmetric CNTRC laminates [0°/90°], and to symmetric CNTRC laminates [0°/90°/0°] and [0°/90°/90°/0°], respectively.

The influence of the side-to-thickness ratio a/h on the nondimensional center deflection of square uniformly distributed and functionally graded CNTRC laminated plate is shown in Fig. 3. Note that the increase of the side-to-thickness ratio leads to a rapid decrement in the nondimensional center deflection for $a/h \leq 15$, then it stabilizes for the higher value. It is clear that the maximum displacement values correspond to the FG-◊ CNTRC

Table 6 Nondimensional* stresses of four-layer CNTRC laminates [0°/90°/90°/0°[(a/h=10, a/b=1)

	Source	$V^*_{cnt}=0.11$				$V^*_{cnt}=0.14$				$V^*_{cnt}=0.17$			
		$\bar{\sigma}_{xx}$	$\bar{\sigma}_{yy}$	$\bar{\tau}_{xy}$	$\bar{\tau}_{xz}$	$\bar{\sigma}_{xx}$	$\bar{\sigma}_{yy}$	$\bar{\tau}_{xy}$	$\bar{\tau}_{xz}$	$\bar{\sigma}_{xx}$	$\bar{\sigma}_{yy}$	$\bar{\tau}_{xy}$	$\bar{\tau}_{xz}$
UD	HSDT	0.6003	0.4117	0.0128	0.0365	0.6159	0.4399	0.0111	0.0362	0.5979	0.4074	0.0131	0.0365
	TSDT	0.5976	0.4136	0.0128	0.0359	0.6127	0.4421	0.0111	0.0357	0.5952	0.4092	0.0131	0.0360
	SSDT	0.6024	0.4101	0.0128	0.0370	0.6185	0.4380	0.0111	0.0367	0.5999	0.4058	0.0131	0.0370
	FSDT	0.5225	0.4184	0.0117	0.0247	0.5211	0.4492	0.0100	0.0245	0.5226	0.4137	0.0120	0.0247
FG-X	HSDT	1.1280	0.7655	0.0139	0.0401	1.1565	0.8151	0.0125	0.0415	1.1271	0.7585	0.0156	0.0438
	TSDT	1.1230	0.7693	0.0139	0.0395	1.1505	0.8197	0.0125	0.0408	1.1223	1.1223	0.7622	0.0156
	SSDT	1.1319	0.7623	0.0139	0.0406	1.1612	0.8113	0.0125	0.0420	1.1309	0.7554	0.0156	0.0444
	FSDT	0.9937	0.7932	0.0129	0.0276	0.9936	0.8507	0.0115	0.0285	0.9980	0.7850	0.0146	0.0301
FG-◊	HSDT	0.0228	0.0126	0.0120	0.0335	0.0188	0.0105	0.0100	0.0321	0.0180	0.0092	0.0114	0.0310
	TSDT	0.0227	0.0126	0.0119	0.0329	0.0187	0.0105	0.0100	0.0315	0.0180	0.0092	0.0114	0.0305
	SSDT	0.0228	0.0125	0.0120	0.0339	0.0188	0.0104	0.0101	0.0325	0.0180	0.0092	0.0114	0.0314
	FSDT	0.0201	0.0129	0.0108	0.0222	0.0162	0.0108	0.0090	0.0213	0.0161	0.0095	0.0103	0.0206
FG-V	HSDT	0.0244	0.0142	0.0141	0.0351	0.0202	0.0119	0.0128	0.0342	0.0193	0.0105	0.0159	0.0336
	TSDT	0.0243	0.0143	0.0141	0.0346	0.0201	0.0119	0.0128	0.0337	0.0192	0.0105	0.0159	0.0331
	SSDT	0.0245	0.0142	0.0141	0.0356	0.0203	0.0118	0.0128	0.0346	0.0193	0.0105	0.0159	0.0340
	FSDT	0.0216	0.0145	0.0130	0.0237	0.0175	0.0122	0.0117	0.0231	0.0173	0.0107	0.0147	0.0227

* Same nondimensionalization as used in Table 3, except $\bar{\sigma}_{yy}$ is evaluated at $(x, y, z) = (a/2, b/2, h/4)$.

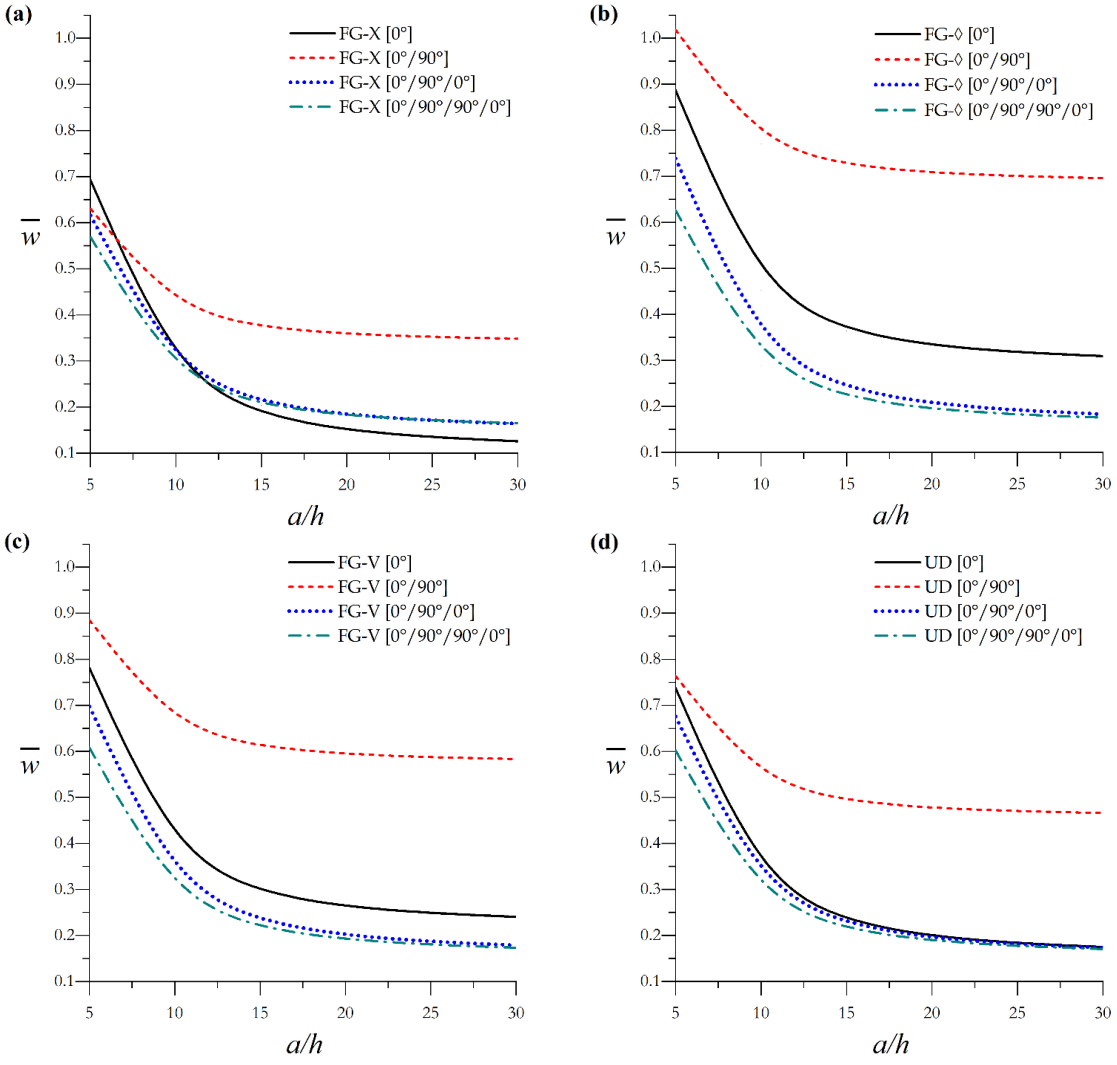

Fig. 3 Effect of side-to-thickness ratio a/h on center deflection of square CNTRC plate; (a): FG-X, (b): FG-◊, (c): FG-V, (d): UD

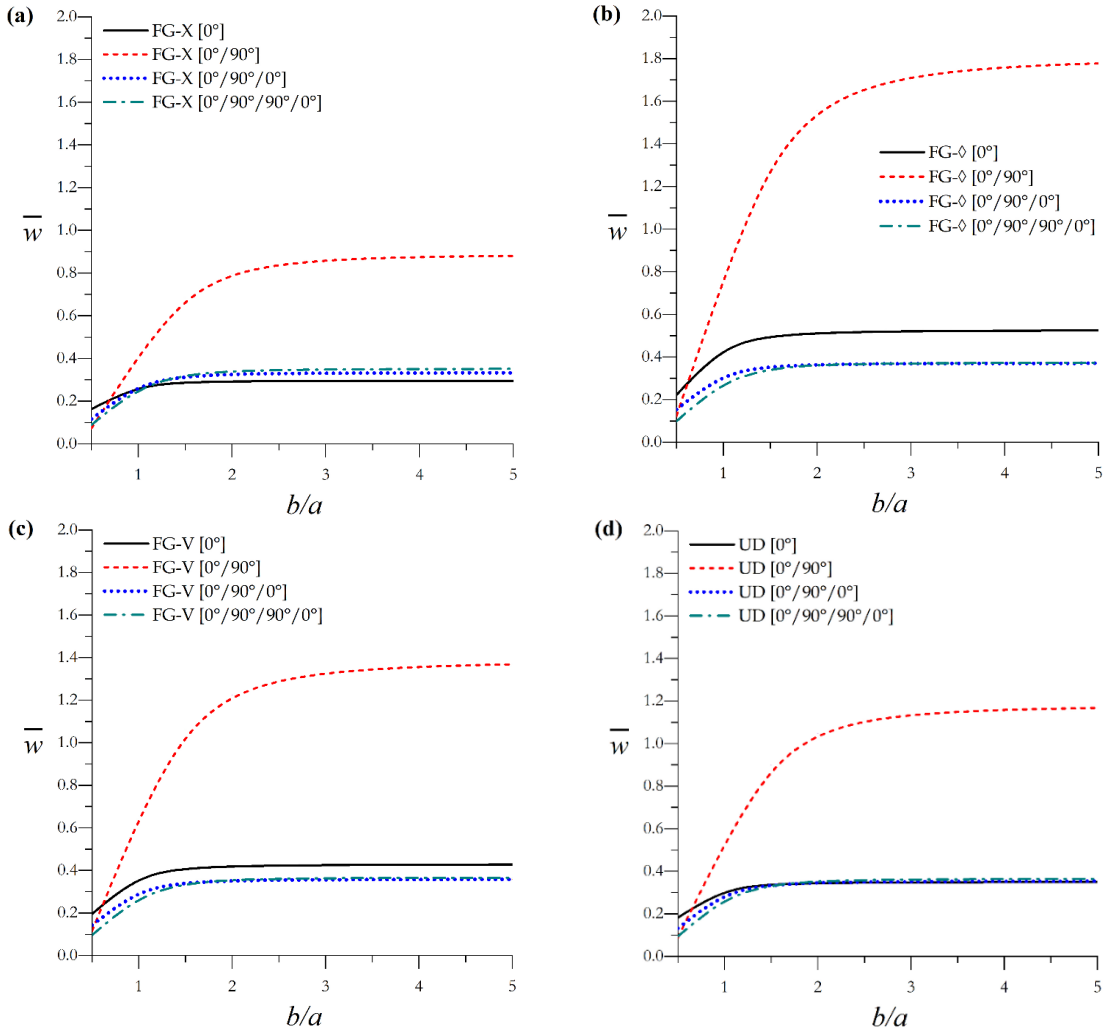

Fig. 4 Effect of aspect ratio b/a on center deflection of CNTRC plate (a=10h); (a): FG-X, (b): FG-◊, (c): FG-V, (d): UD

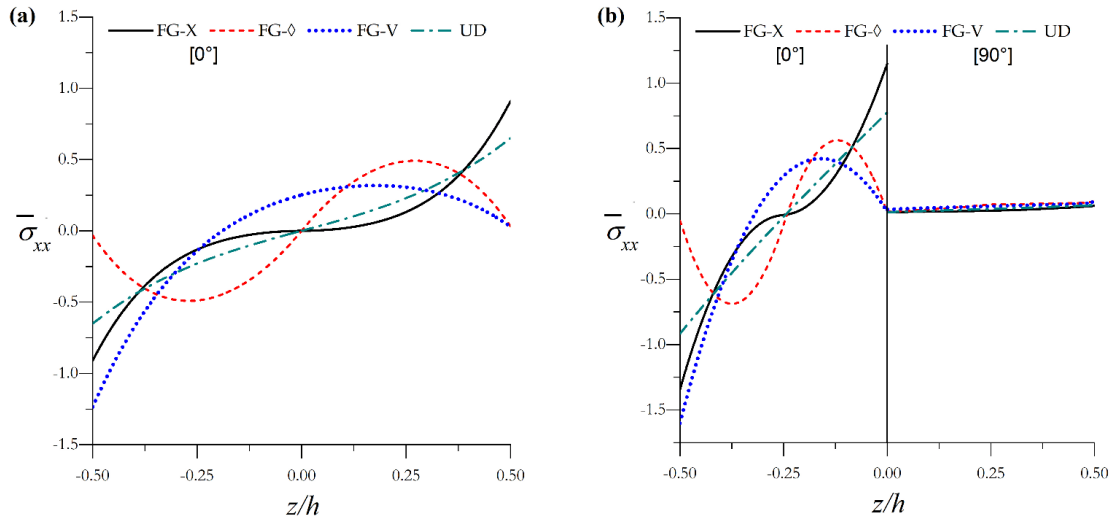

Fig. 5 Dimensionless stresses $\bar{\sigma}_{xx}$ of CNTRC square plates

laminated plates, especially in the case of a [0°, 90°] CNTRC laminated plate.

In Fig. 4, nondimensional center deflection of the CNTRC laminated plate versus the aspect ratio b/a is presented. It can be observed that the dimensionless center deflection increases with the increase of the aspect ratio increase just for $b/a \leq 2$, wherever the reinforcement material distributions are, then it stabilizes when the aspect ratio reaches its highest value.

Generally, the laminated plates [0°/90°] have the largest

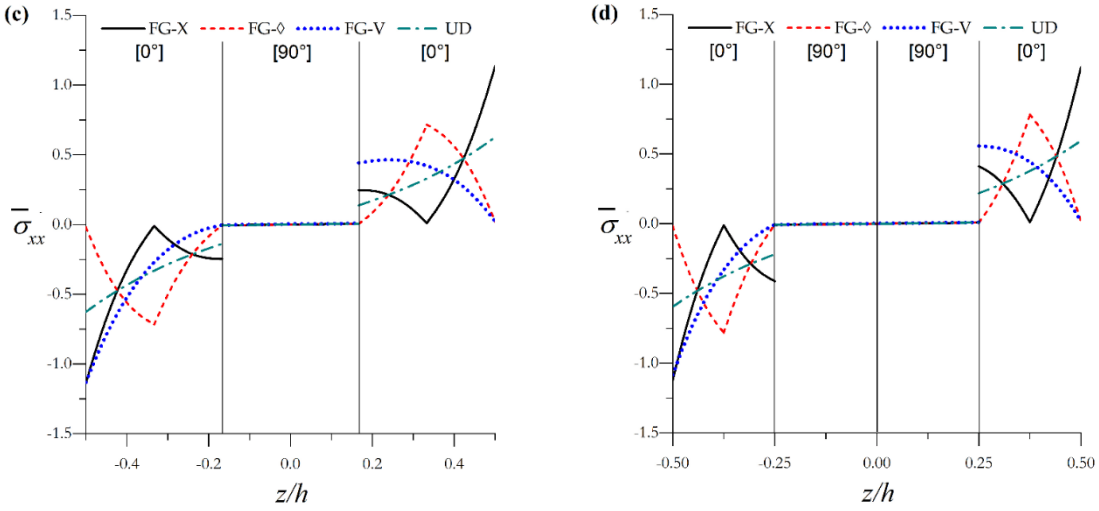

Fig. 5 Continued

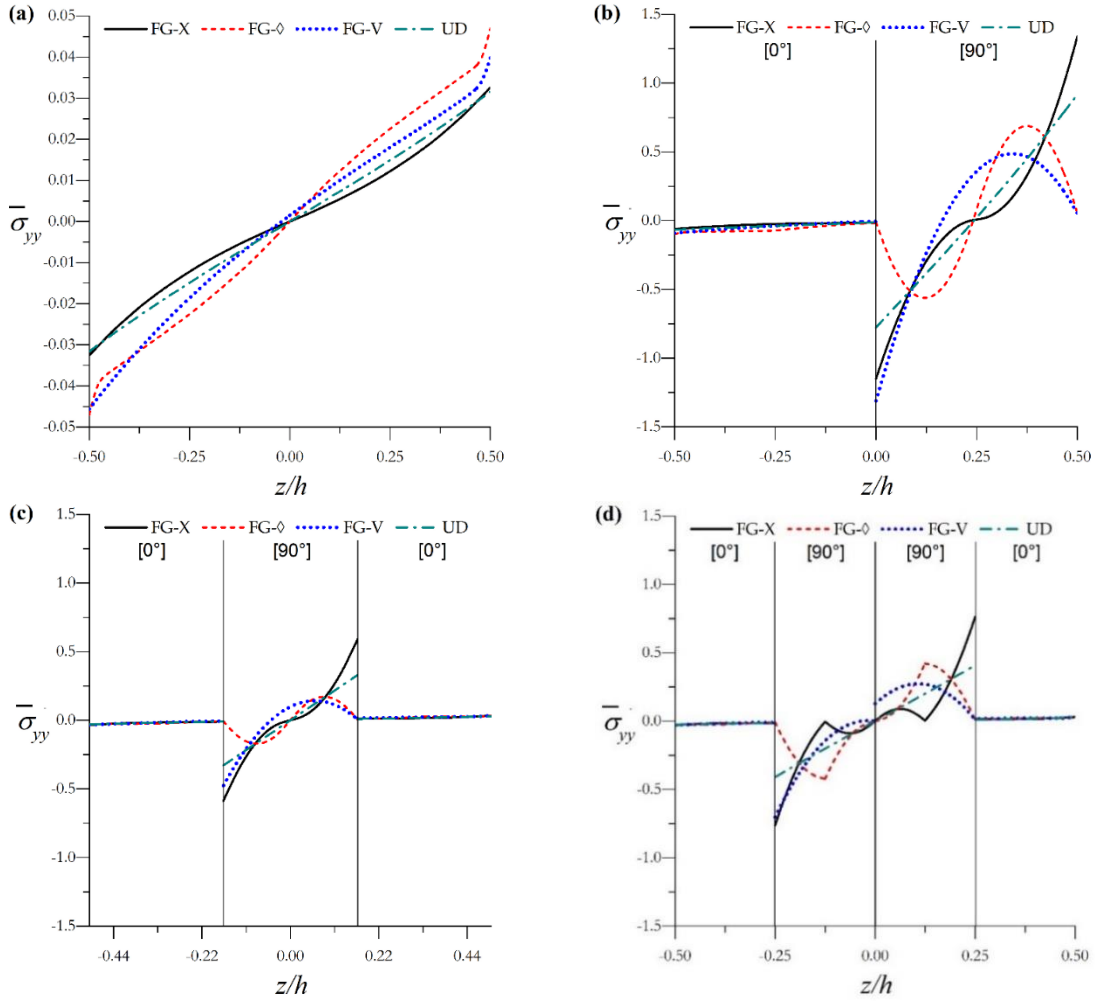

Fig. 6 Dimensionless stresses $\bar{\sigma}_{yy}$ of CNTRC square plates

transverse displacement, which means that they are characterized by a lower resistance to the transverse than the other laminated composite plates. Also, it can be concluded that the use of CNTRC laminates can help to ameliorate the strength and stiffness of engineered structures.

To clearly understand normal stresses and shear stresses variations in CNTRC square plates with $a/h = 10$, Figs. 5 to 8 show the plots of the results across the plate thickness with different CNT distribution patterns and different CNT volume fraction values. According to these figures, all plotted stress results are symmetric about the middle plane

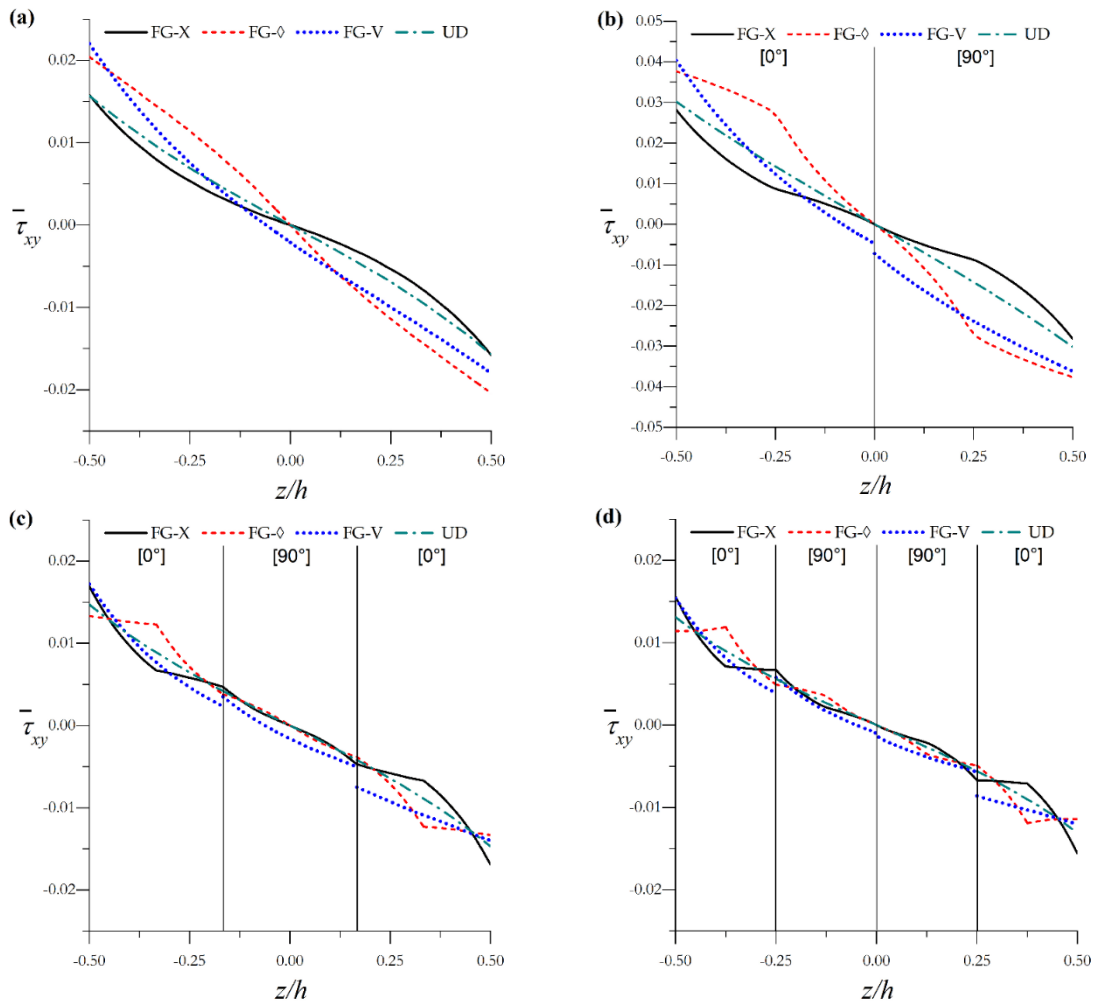

Fig. 7 Dimensionless stresses $\bar{\tau}_{xy}$ of CNTRC square plates

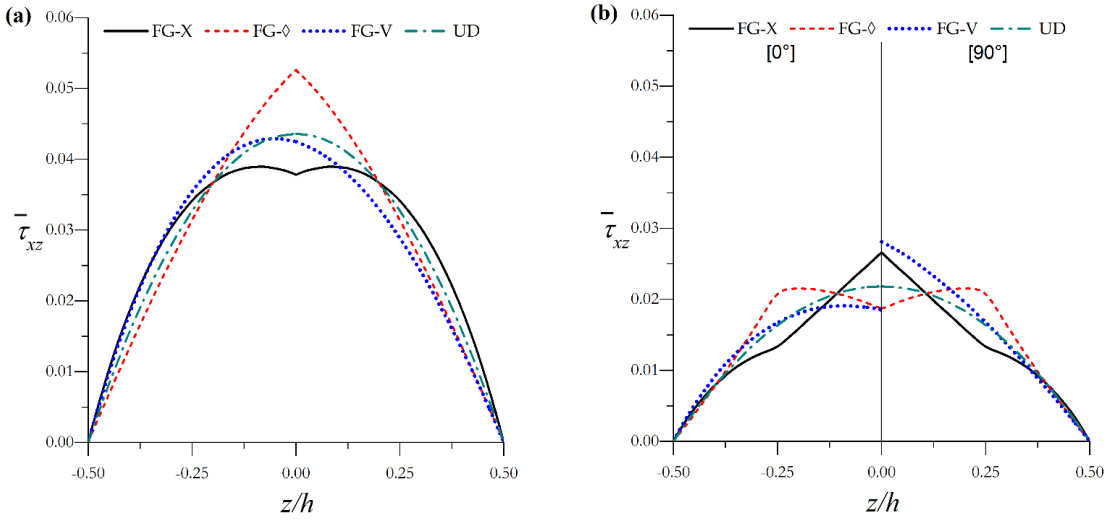

Fig. 8 Dimensionless stresses $\bar{\tau}_{xz}$ of CNTRC square plates

z=0 for the single layer [0°] plate and the two symmetric layered [0°/90°/0°] and [0°/90°/90°/0°] laminated plates, except for FG-V CNTRC plates, which have unsymmetrical reinforcement distributions

In Fig. 5, dimensionless normal stresses $\bar{\sigma}_{xx}$ through the thickness of various CNTRC laminated plates are plotted. For the FG-◊ CNTRC laminated plate, having zeroth carbon nanotubes on the top and bottom layer surfaces (see Fig. 2), the normal stresses $\bar{\sigma}_{xx}$ are continuous at the laminate interfaces, whereas the stresses $\bar{\sigma}_{xx}$ for the other types of CNTRC laminated plates are discontinuous at the interfaces. Moreover, the normal

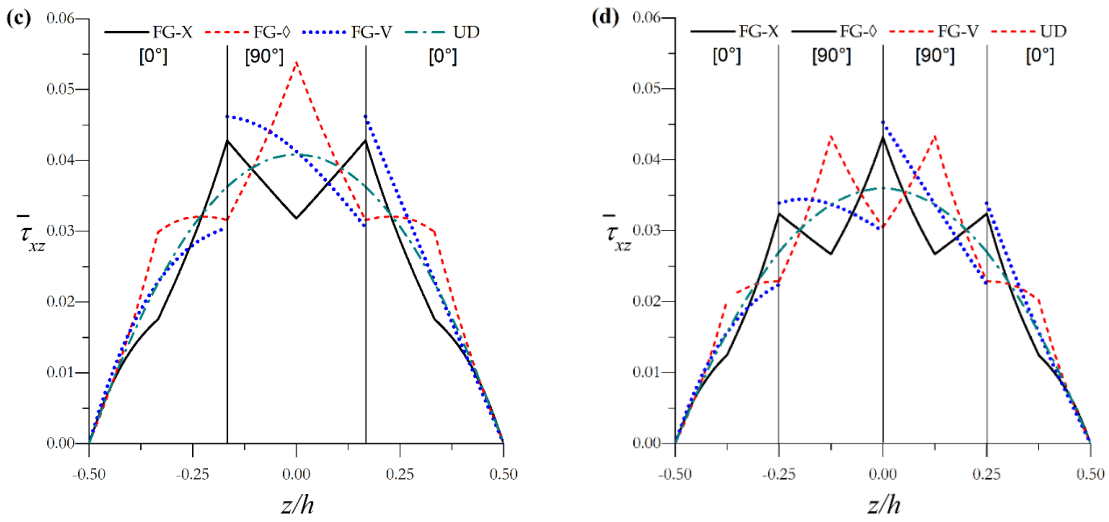

Fig. 8 Continued

stresses have a large value for the [0°] lamina than that for the [90°] lamina, wherever the composite structure is.

Fig. 6 illustrates the variation of stresses $\bar{\sigma}_{yy}$through the thickness direction of CNTRC square plates. The highest values of stresses $\bar{\sigma}_{yy}$are is detected for [90°] layers which have the same direction of carbon nanotubes.

Fig. 7 demonstrates the distribution of dimensionless shear stresses $\bar{\tau}_{xy}$ along the thickness of CNTRC square plates. It is clear that the highest values of $\bar{\tau}_{xy}$ refer to [0°/90°] CNTRC laminated plates. The compressive and tensile values of CNTRC plate stresses $\bar{\tau}_{xy}$ are maximum at the top and the bottom surfaces.

Fig. 8 shows the variation of dimensionless stresses $\bar{\tau}_{xz}$ across the CNTRC square plate thickness. The maximum value of stresses $\bar{\tau}_{xz}$ occurs at a point on the mid-plane for the UD CNTRC laminated plate, which has a continuous and smooth variation. It is worth to note that the variation of stresses $\bar{\tau}_{xz}$ is related to the reinforcement material distribution, if the stresses $\bar{\tau}_{xz}$ of each layer of the laminate (Fig. 8) is compared with the distribution of the CNTs in Fig. 2.

6. Conclusions

In the current article, the bending behavior of cross-ply single-walled carbon nanotube-reinforced composite laminated plates, subjected to sinusoidal loading, is investigated. Several numerical results are carried out to investigate transverse displacement and stresses of four types of reinforcement material distributions, a uniform distribution UD and three functionally graded (FG) distributions, through the layer thickness. Various shear deformation theories are used to derive the field equations of simply supported CNTRC laminated plates.

Numerical computations are carried out to show the influence of the side-to-thickness a/h, the aspect ratio b/a, the carbon nanotube volume fraction and the laminated composite structure on the stresses and the transverse displacement.

In conclusion, carbon nanotube reinforcement and laminated composite type play an important role in determining the static response of the CNTRC laminated plates.

The analysis derived herein may be useful in further research and should provide engineers with the capability of designing CNTRC plates for special technical implementations.

Acknowledgment

This research was supported by the Algerian Directorate General of Scientific Research and Technological Development (DGRSDT) and University of Mustapha Stambouli of Mascara (UMS
Mascara) in Algeria.

References

Alibeigloo, A. (2013), "Static analysis of functionally graded carbon nanotube-reinforced composite plate embedded in piezoelectric layers by using theory of elasticity", *Compos. Struct.*, **95**, 612-622. https://doi.org/10.1016/j.compstruct.2017.06.015.

Alibeigloo, A. and Liew, K.M. (2013), "Thermoelastic analysis of functionally graded carbon nanotube-reinforced composite plate using theory of elasticity", *Compos. Struct.*, **106**, 873-881. https://doi.org/10.1016/j.compstruct.2013.07.002.

Ansari, R., Hasrati, E., Faghih Shojaei, M., Gholami, R. and Shahabodini, A. (2015), "Forced vibration analysis of functionally graded carbon.nanotube-reinforced composite plates using a numerical strategy", *Physica E: Low Dimens. Syst. Nanostruct.*, **69**, 294-305. https://doi.org/10.1016/j.physe.2015.01.011.

Bakhadda, B., Bachir-Bouiadjra, M., Bourada, F., Bousahla, A.A., Tounsi, A. and Mahmoud SR. (2018), "Dynamic and bending analysis of carbon nanotube-reinforced composite plates with elastic foundation", *Wind Struct.*, **27**, 311-324. https://doi.org/10.12989/was.2018.27.5.311.

Batou, B., Nebab, M., Bennai, R., AitAtmane, H., Tounsi, A., Bouremana, M. (2019), "Wave dispersion properties in

imperfect sigmoid plates using various HSDTs", *Steel Compos. Struct.*, **33**(5), 699-716. https://doi.org/10.12989/scs.2019.33.5.699.

Belmahi, S., Zidour, M. and Meradjah, M. (2019), "Small-scale effect on the forced vibration of a nano beam embedded an elastic medium using nonlocal elasticity theory", *Adv. Aircraft Spacecraft Sci.*, **6**(1), 1-18. http://dx.doi.org/10.12989/aas.2019.6.1.001.

Bensattalah, T., Zidour, M. and Daouadji, T.H. (2018), "Analytical analysis for the forced vibration of CNT surrounding elastic medium including thermal effect using nonlocal Euler-Bernoulli theory", *Adv. Mater. Res.*, **7**(3), 163-174. https://doi.org/10.12989/amr.2018.7.3.163.

Bensattalah, T., Zidour, M. and Daouadji, T.H. (2019), "A new nonlocal beam model for free vibration analysis of chiral single-walled carbon nanotubes", *Compos. Mater. Eng.*, **1**(1), 21-31. https://doi.org/10.12989/cme.2019.1.1.021.

Boulal, A., Bensattalah, T., Karas, A., Zidour, M., Heireche, H. and Bedia, E.A. (2020), "Buckling of carbon nanotube reinforced composite plates supported by Kerr foundation using Hamilton's energy principle", *Struct. Eng. Mech.*, **73**(2), 209. https://doi.org/10.12989/sem.2020.73.2.209.

Chelahi, C.S., Kaci, A., Bousahla, A. A., Tounsi, A., Benrahou, K. H. and Tounsi, A. (2020), "A novel four-unknown integral model for buckling response of FG sandwich plates resting on elastic foundations under various boundary conditions using Galerkin's approach", *Geomech. Eng.*, **21**(5), 471-487. https://doi.org/10.12989/gae.2020.21.5.471

Daikh, A.A. and Zenkour, A.M. (2019a), "Effect of porosity on the bending analysis of various functionally graded sandwich plates", *Mater. Res. Expres.*, **6**, 065703.

Daikh, A.A. and Zenkour, A.M. (2019b), "Free vibration and buckling of porous power-law and sigmoid functionally graded sandwich plates using a simple higher-order shear deformation theory", *Mater. Res. Express*, **6**(11) 115707. https://doi.org/10.1088/2053-1591/ab48a9

Daikh, A.A. Bachiri, A. Houari, M.S.A. and Tounsi, A. (2020b), "Size dependent free vibration and buckling of multilayered carbon nanotubes reinforced composite nanoplates in thermal environment", *Mech. Bas. Des. Struct. Mach.*, 1-29. https://doi.org/10.1080/15397734.2020.1752232.

Daikh, A.A., Drai, A., Bensaid, I., Houari, M.S.A. and Tounsi, A. (2020), "On vibration of functionally graded sandwich nanoplates in the thermal environment", *J. Sandw. Struct. Mater.*, 1099636220909790. https://doi.org/10.1177/1099636220909790.

Draoui. A., Zidour, M., Tounsi, A. and Adim, B. (2019), "Static and dynamic behavior of nanotubes-reinforced sandwich plates using (FSDT)", *J. Nano Res.*, **57**, 117-135. https://doi.org/10.4028/www.scientific.net/JNanoR.57.117.

Esawi, A.M.K. and Farag, M.M. (2007), "Carbon nanotube reinforced composites: potential and current challenges", *Mater. Des.*, **2**, 394-401. https://doi.org/10.1016/j.matdes.2006.09.022.

Fazzolari, F.A. (2018), "Thermoelastic vibration and stability of temperature-dependent carbon nanotube-reinforced composite plates", *Compos. Struct.*, **196**, 199-214. https://doi.org/10.1016/j.compstruct.2018.04.026.

Fidelus, J.D., Wiesel, E., Gojny, F.H., Schulte, K. and Wagner, H.D. (2005), "Thermo-mechanical properties of randomly oriented carbon/epoxy nanocomposites", *Compos.: Part A*, **36**, 1555-1561. https://doi.org/10.1016/j.compositesa.2005.02.006.

Griebel, M. and Hamaekers, J. (2004), "Molecular dynamics simulations of the elastic moduli of polymer-carbon nanotube composites", *Comput. Meth. Appl. Mech. Eng.*, **193**, 1773-1788. https://doi.org/10.1016/j.cma.2003.12.025.

Guessas, H., Zidour, M., Meradjah, M. and Tounsi, A. (2018), "The critical buckling load of reinforced nanocomposite porous plates", *Struct. Eng. Mech.*, **67**, 115-123. https://doi.org/10.12989/sem.2018.67.2.115.

Han, Y. and Elliott, J. (2007), "Molecular dynamics simulations of the elastic properties of polymer/carbon nanotube composites", *Comput. Mater. Sci.*, **39**, 315-23. https://doi.org/10.1016/j.commatsci.2006.06.011.

Kaci, A., Tounsi, A., Bakhti, K. and Adda Bedia, E.A. (2012), "Nonlinear cylindrical bending of functionally graded carbon nanotube-reinforced composite plates", *Steel Compos. Struct.*, **12**, 491-504. https://doi.org/10.12989/scs.2012.12.6.491.

Karama, M., Afaq, K.S. and Mistou, S. (2009), "A new theory for laminated composite plates", *Proc. Inst. Mech. Eng., Part L: J. Mater. Des. Appl.*, **223**, 53-62. https://doi.org/10.1243/14644207JMDA189.

Karami, B., Janghorban, M. and Li, L. (2018a), "On guided wave propagation in fully clamped porous functionally graded nanoplates", *Acta Astronautica*, **143**, 380-390. https://doi.org/10.1016/j.actaastro.2017.12.011.

Karami, B., Janghorban, M. and Rabczuk, T. (2019a), "Analysis of elastic bulk waves in functionally graded triclinic nanoplates using a quasi-3D bi-Helmholtz nonlocal strain gradient model", *Eur. J. Mech.-A/Solid.*, **78**, 103822. https://doi.org/10.1016/j.euromechsol.2019.103822.

Karami, B., Janghorban, M. and Rabczuk, T. (2020a), "Forced vibration analysis of functionally graded anisotropic nanoplates resting on wWinkler/Pasternak-Foundation", *Comput. Mater. Continua*, **62**(2), 607-629. http://dx.doi.org/10.32604/cmc.2020.08032.

Karami, B., Janghorban, M., Shahsavari, D. and Tounsi, A. (2018b), "A size-dependent quasi-3D model for wave dispersion analysis of FG nanoplates", *Steel Compos. Struct.*, **28**, 99-110. http://dx.doi.org/10.12989/scs.2018.28.1.099.

Karami, B., Shahsavari, D. and Janghorban, M. (2018), "A Comprehensive analytical study on functionally graded carbon nanotube-reinforced composite plates", *Aerosp. Sci. Technol.*, **82**, 499-512. https://doi.org/10.1016/j.ast.2018.10.001.

Karami, B., Shahsavari, D., Janghorban, M. and Li, L. (2019b), "Elastic guided waves in fully-clamped functionally graded carbon nanotube-reinforced composite plates", *Mater. Res. Express*, **6**(9), 0950a9.

Karami, B., Shahsavari, D., Janghorban, M. and Li, L. (2020b), "Free vibration analysis of FG nanoplate with poriferous imperfection in hygrothermal environment", *Struct. Eng. Mech.*, **73**(2), 191-207. http://dx.doi.org/10.12989/sem.2020.73.2.191.

Kiani, Y. (2016), "Free vibration of functionally graded carbon nanotube reinforced composite plates integrated with piezoelectric layers", *Comput. Math. Appl.*, **72**, 2433-2449. https://doi.org/10.1016/j.camwa.2016.09.007.

Lau, K.T., Gu, C., Gao, G.H., Ling H.Y. and Reid, S.R. (2004), "Stretching process of single- and multiwalled carbon nanotubes for nanocomposite applications", *Carbon*, **42**, 426-8.

Lei, X.Z., Liew, K.M. and Yu, J.L. (2013), "Buckling analysis of functionally graded carbon nanotube-reinforced composite plates using the element-free kp-Ritz method", *Compos. Struct.*, **98**, 160-168. https://doi.org/10.1016/j.compstruct.2012.11.006.

Lei, X.Z., Liew, K.M. and Yu, J.L. (2013), "Free vibration analysis of functionally graded carbon nanotube-reinforced composite plates using the element-free kp-Ritz method in thermal environment", *Compos. Struct.*, **106**, 128-138. https://doi.org/10.1016/j.compstruct.2013.06.003.

Lei, X.Z., Liew, K.M. and Yu, J.L. (2013), "Large deflection analysis of functionally graded carbon nanotube reinforced composite plates by the element-free kp-Ritz method", *Comput. Meth. Appl. Mech. Eng.*, **256**, 189-199. https://doi.org/10.1016/j.cma.2012.12.007.

Mehar, K. and Panda, S.K. (2018), "Elastic bending and stress analysis of carbon nanotube-reinforced composite plate: Experimental, numerical, and simulation", *Adv. Polym. Technol.*, **37**, 1643-1657. https://doi.org/10.1002/adv.21821.

Mirzaei, M. and Kiani, Y. (2016), "Free vibration of functionally graded carbon-nanotube-reinforced composite plates with cutout", *Beilstein J. Nanotechnol.*, **7**, 511-523. https://doi.org/10.3762/bjnano.7.45.

Natarajan, S., Haboussi, M. and Manickam, G. (2014), "Application of higher-order structural theory to bending and free vibration analysis of sandwich plates with CNT reinforced composite facesheets", *Compos. Struct.*, **113**, 197-207. https://doi.org/10.1016/j.compstruct.2014.03.007.

Phung-Van, P., Abdel-Wahab, M. and Liew, K.M., Bordas, S.P.A. and Nguyen-Xuan, H. (2015), "Isogeometric analysis of functionally graded carbon nanotube-reinforced composite plates using higher-order shear deformation theory", *Compos. Struct*., **123**, 137-149. https://doi.org/10.1016/j.compstruct.2014.12.021.

Rafiee, M., He, X.Q. and Liew, K.M. (2014), "Non-linear dynamic stability of piezoelectric functionally graded carbon nanotube-reinforced composite plates with initial geometric imperfection", *Int. J. Nonlin. Mech.*, **59**, 37-45. https://doi.org/10.1016/j.ijnonlinmec.2013.10.011.

Reddy, J.N. (1984), "A simple higher-order theory for laminated composite plates", *J. Appl. Mech.*, **51**, 745-752.

Salah, F., Boucham, B., Bourada, F., Benzair, A., Bousahla, A.A., Tounsi, A. (2019), "Investigation of thermal buckling properties of ceramic-metal FGM sandwich plates using 2D integral plate model", *Steel Compos. Struct.*, **33**(6), 805-822. https://doi.org/10.12989/scs.2019.33.6.805.

Shahsavari, D., Karami, B. and Janghorban, M. (2019), "On buckling analysis of laminated composite plates using a nonlocal refined four-variable model", *Steel Compos. Struct.*, **32**(2), 173-187. http://dx.doi.org/10.12989/scs.2019.32.2.173.

Shahsavari, D., Shahsavari, M., Li, L. and Karami, B. (2018), "A novel quasi-3D hyperbolic theory for free vibration of FG plates with porosities resting on Winkler/Pasternak/Kerr foundation", *Aerosp. Sci. Technol.*, **72**, 134-149. https://doi.org/10.1016/j.ast.2017.11.004.

Shams, S.H., Soltani, B. and MemarArdestani, M. (2016), "The effect of elastic foundations on the buckling behavior of functionally graded carbon nanotube-reinforced composite plates in thermal environments using a meshfree method", *J. Solid Mech.*, **8**, 262-279.

Shen, H.S. (2009), "Nonlinear bending of functionally graded carbon nanotube-reinforced composite plates in thermal environments", *Compos. Struct*., **91**, 9-19. https://doi.org/10.1016/j.compstruct.2009.04.026.

Shen, H.S. and Zhang, C.L. (2010), "Thermal buckling and postbuckling behavior of functionally graded carbon nanotube-reinforced composite plates", *Mater. Des*., **31**, 3403-3411. https://doi.org/10.1016/j.matdes.2010.01.048.

Thai, C.H., Ferreira, A.J.M. and Rabczuk, T. and Nguyen-Xuan, H.A (2017), "A naturally stabilized nodal integration meshfree formulation for carbon nanotube-reinforced composite plate analysis", *Eng. Anal. Bound. Elem.*, **92**, 136-155. https://doi.org/10.1016/j.enganabound.2017.10.018.

Touratier, M. (1991), "An efficient standard plate theory", *Int. J. Eng. Sci.*, **29**, 901-916. https://doi.org/10.1016/0020-7225(91)90165-Y.

Trang, L.T.N. and Tung, H.V. (2018), "Tangential edge constraint sensitivity of nonlinear stability of CNT-reinforced composite plates under compressive and thermomechanical loadings", *J. Eng. Mech.*, ASCE, **144**, 04018056. https://doi.org/10.1061/(ASCE)EM.1943-7889.0001479.

Truong-Thi, T., Vo-Duy, T., Ho-Huu, V. and Nguyen-Thoi, T. (2018), "Static and free vibration analyses of functionally graded carbon nanotube reinforced composite plates using CS-DSG3", *Int. J. Comput. Meth.*, **17**, 1850133. https://doi.org/10.1142/S0219876218501335.

Vodenitcharova, T. and Zhang, L.C. (2003), "Effective wall thickness of a single-walled carbon nanotube", *Phys. Rev. B*, **68**, 165401. https://doi.org/10.1103/PhysRevB.68.165401.

Wang, Z.X. and Shen, H.S. (2011), "Nonlinear vibration of nanotube-reinforced composite plates in thermal environments", *Comput. Mater. Sci.*, **50**, 2319-2330. https://doi.org/10.1016/j.commatsci.2011.03.005.

Wang, Z.X. and Shen, H.S. (2012), "Nonlinear dynamic response of nanotube-reinforced composite plates resting on elastic foundations in thermal environments", *Nonlin. Dyn.*, **70**, 735-754. https://doi.org/10.1007/s11071-012-0491-2.

Wattanasakulpong, N. and Chaikittiratana, A. (2015), "Exact solutions for static and dynamic analyses of carbon nanotube-reinforced composite plates with Pasternak elastic foundation", *Appl. Math. Model.*, **39**, 5459-5472. https://doi.org/10.1016/j.apm.2014.12.058.

Zamani Nejad, M. and Taghizadeh, T. (2017), "Elastic analysis of carbon nanotube-reinforced composite plates with piezoelectric layers using shear deformation theory", *Int. J. Appl. Mech.*, **9**, 1750011. https://doi.org/10.1142/S1758825117500119.

Zhang, L.W. and Liew, K.M. (2015), "Geometrically nonlinear large deformation analysis of functionally graded carbon nanotube reinforced composite straight-sided quadrilateral plates", *Comput. Meth. Appl. Mech. Eng*., **295**, 219-239. https://doi.org/10.1016/j.cma.2015.07.006.

Zhang, L.W., Cui, W.C. and Liew, K.M. (2015), "Vibration analysis of functionally graded carbon nanotube reinforced composite thick plates with elastically restrained edges", *Int. J. Mech. Sci.*, **103**, 9-21. https://doi.org/10.1016/j.ijmecsci.2015.08.021.

Zhu, P., Lei, Z.X. and Liew, K.M. (2012), "Static and free vibration analyses of carbon nanotube-reinforced composite plates using finite element method with first order shear deformation plate theory", *Compos. Struct*., **94**, 1450-1460. https://doi.org/10.1016/j.compstruct.2011.11.010.

Zhu, R., Pan, E. and Roy, A.K. (2007), "Molecular dynamics study of the stress-strain behavior of carbon-nanotube reinforced Epon 862 composites", *Mater. Sci. Eng A*, **447**, 51-57. https://doi.org/10.1016/j.msea.2006.10.054.

HK